

Cyclotron resonance in mercury: Temperature dependence and the electron-phonon interaction*

Sung Ho Choh

Department of Physics, McMaster University, Hamilton, Ontario, Canada

Department of Physics, Korea University, Seoul, Korea[†]

W. R. Datars

Department of Physics, McMaster University, Hamilton, Ontario, Canada

(Received 4 June 1973)

The temperature dependence of the effective cyclotron mass and the electronic relaxation time in mercury have been investigated by Azbel'-Kaner cyclotron resonance using a microwave frequency of 35 GHz. The measurements cover the temperature range 1.15 to 2.5 K in 0.05-K intervals. Two orbits are studied with the magnetic field in the binary-bisectrix crystallographic plane of the sample surface. For both orbits, the cyclotron mass m^* is found to increase as the temperature squared, in good agreement with the prediction of the theory of the electron-phonon interaction. The relative mass increments at 2.5 K with respect to 0 K are 4.2% for one orbit and 3.6% for another. These different values indicate that the effect is dependent upon the cyclotron orbits, and are discussed in terms of a directional phonon spectrum. The experimental relaxation rate varies more rapidly than the cube of the temperature. The variation is found to be proportional to $T^{5.2 \pm 0.3}$, which confirms previous experimental results, and indicates that the low-energy portion of the $\alpha^2(\omega)F(\omega)$ spectrum is nonquadratic.

I. INTRODUCTION

The experimentally observed cyclotron mass m^* of many metals at low temperature is generally larger than the mass calculated from the band structure. This discrepancy is mainly attributed to the electron-phonon interaction,¹ making many-body effects observable in cyclotron resonance.² Since the energy of a quasiparticle measured near the Fermi level depends on the electron-phonon interaction strength, the cyclotron effective mass m^* and electronic relaxation time τ are dependent on the frequency and temperature of the cyclotron-resonance experiments. The frequency dependence of the effect on m^* has been discussed by Scher and Holstein.³ Grimvall⁴ has predicted that m^* and τ in mercury and lead have a significant variation with frequency and temperature. These are materials with a strong electron-phonon interaction.

Experiments on mercury have shown that m^* and τ change with temperature⁵ and frequency.⁶ Other measurements have indicated changes of m^* with frequency in lead,⁶ with temperature in zinc⁷ and lead,⁸ and changes of m^* and τ with frequency and temperature in lead⁹ and indium.¹⁰ Previous theories^{4,11} have mainly considered the Fermi surface (FS) average of the phonon spectrum in calculating the temperature effect. However, the experimental results of zinc⁷ and the present study of mercury give evidence that the temperature dependence of m^* does depend on the electronic orbit. The anisotropy of the mass change in zinc for different orbits with temperature has been ex-

plained by Truant and Carbotte,¹² using the anisotropy of the phonon spectrum.

The purpose of the present study is to present the results of an Azbel'-Kaner¹³ cyclotron-resonance experiment, which measured the temperature dependence of the cyclotron effective mass m^* and of the electronic relaxation time τ in mercury. The measurements were performed at a fixed frequency of 35 GHz and at temperatures between 1.1 and 2.5 K for two orbits. Cyclotron resonance was not observable at temperatures above 2.5 K, where the temperature-dependent relaxation time was too small. Preliminary results of this work on the temperature dependence of m^* and τ have been reported previously.^{14,15}

II. THEORY OF ELECTRON-PHONON INTERACTION

A. Electron-phonon interaction at 0 K

In cyclotron-resonance experiments, a cyclotron mass $m^*(O_{\mathbf{k}})$ characteristic of an orbit $O_{\mathbf{k}}$ perpendicular to \mathbf{k} is measured. This experimental cyclotron mass m^* is usually larger than the band mass m_b . This discrepancy is attributed to the electron-phonon interaction¹ and the electron-electron interaction.

In the absence of electron-phonon and electron-electron interactions, the mass can be expressed in terms of the band structure $\epsilon_{\mathbf{k}}$ ¹¹:

$$m_b(O_{\mathbf{k}}) = \frac{\hbar^2}{2\pi} \oint \frac{dl}{n_{\mathbf{k}} \cdot \nabla_{\mathbf{k}} \epsilon_{\mathbf{k}}}, \quad (1)$$

where $n_{\mathbf{k}}$ is a unit vector at \mathbf{k} normal to the orbit in the plane perpendicular to the magnetic field,

dl is a line element in \mathbf{k} space, and the integral is evaluated around the orbit $O_{\mathbf{k}}$ on the Fermi surface. The presence of the electron-phonon interaction modifies the energy of an electron near the FS, and the new energy $E_{\mathbf{k}}$ of a quasiparticle in an orbit $O_{\mathbf{k}}$ is the sum of the single-particle energy $\epsilon_{\mathbf{k}}$ and the complex electron self-energy $\Sigma_{e1\text{ph}}$ due to the electron-phonon interaction:

$$\begin{aligned} E_{\mathbf{k}} &= \epsilon_{\mathbf{k}} + \Sigma_{e1\text{ph}}(\mathbf{k}, E_{\mathbf{k}}) \\ &= \epsilon_{\mathbf{k}} + M_{e1\text{ph}}(\mathbf{k}, E_{\mathbf{k}}) - i\Gamma_{e1\text{ph}}(\mathbf{k}, E_{\mathbf{k}}). \end{aligned} \quad (2)$$

The real part $M_{e1\text{ph}}$ of the complex self-energy gives the mass enhancement and the imaginary part $\Gamma_{e1\text{ph}}$ gives the quasiparticle lifetime, as discussed below.

The renormalized cyclotron mass m^* is given by

$$m^*(O_{\mathbf{k}}) = \frac{\hbar^2}{2\pi} \oint \frac{dl}{n_{\mathbf{k}} \cdot \nabla_{\mathbf{k}} E_{\mathbf{k}}} \quad (3)$$

instead of Eq. (1). Then the mass renormalization coefficient $\lambda(O_{\mathbf{k}})$ is defined by

$$m^*(O_{\mathbf{k}}) = [1 + \lambda(O_{\mathbf{k}})] m_b(O_{\mathbf{k}}). \quad (4)$$

From Eqs. (1), (3), and (4) we get

$$\lambda(O_{\mathbf{k}}) = \frac{\oint (\lambda_{\mathbf{k}} dl / n_{\mathbf{k}} \cdot \nabla_{\mathbf{k}} \epsilon_{\mathbf{k}})}{\oint (dl / n_{\mathbf{k}} \cdot \nabla_{\mathbf{k}} \epsilon_{\mathbf{k}})}, \quad (5)$$

where $\lambda_{\mathbf{k}}$ is related to $M_{e1\text{ph}}$ by

$$\lambda_{\mathbf{k}} = -\frac{\partial}{\partial \omega} [M_{e1\text{ph}}(\mathbf{k}, \omega)]_{E_F}. \quad (6)$$

Therefore, $\lambda(O_{\mathbf{k}})$ is a function of the orbit $O_{\mathbf{k}}$ under consideration.

The general information of the electron-phonon interaction can be extracted out of the $\alpha^2(\omega)F(\omega)$ function, experimentally determined by the superconducting-tunneling technique.¹⁶ $\alpha(\omega)$ is the electron-phonon coupling constant and $F(\omega)$ is the phonon density of states. The experimental $\alpha^2(\omega)F(\omega)$ is actually the FS average of the $\alpha_{\mathbf{k}}^2(\omega)F_{\mathbf{k}}(\omega)$,

$$\alpha^2(\omega)F(\omega) = \int_{\text{FS}} \frac{d\Omega_{\mathbf{k}}}{4\pi} \alpha_{\mathbf{k}}^2(\omega) F_{\mathbf{k}}(\omega), \quad (7)$$

and is in general different from the directional $\alpha_{\mathbf{k}}^2(\omega)F_{\mathbf{k}}(\omega)$. Likewise, the FS average of the $\lambda(O_{\mathbf{k}})$ can be determined and is given by¹⁶

$$\lambda_0(T=0) = 2 \int_0^{\infty} \frac{d\omega}{\omega} \alpha^2(\omega)F(\omega). \quad (8)$$

λ_0 and $\lambda(O_{\mathbf{k}})$ are not the same because λ_0 is no longer dependent on the orbit $O_{\mathbf{k}}$. Large values of λ_0 are found in two strong-coupling superconduc-

tors¹⁶: $\lambda_0 = 1.6$ for mercury, the largest value for any metal, and $\lambda_0 = 1.5$ for lead.

B. Electron-phonon interaction at finite temperature

The electron-phonon interaction distorts the band structure $E_{\mathbf{k}}$ relative to the single-particle band structure $\epsilon_{\mathbf{k}}$. As the temperature increases, the distortion of $E_{\mathbf{k}}$ changes and, consequently, the cyclotron mass and relaxation time depend on temperature. Experimentally, the changes of the electron-phonon interaction with temperature are more interesting than the electron-phonon interaction at zero temperature. The first-order formula for the self-energy at finite temperature is⁴

$$\begin{aligned} \Sigma(\mathbf{k}, \epsilon_{\mathbf{k}}) &= \hbar \int d\epsilon' \int d\omega' \alpha_{\mathbf{k}}^2(\omega') F_{\mathbf{k}}(\omega') \\ &\times \left(\frac{1 - f(\epsilon') + N(\omega')}{\epsilon - \epsilon' - \hbar\omega' + i\delta} + \frac{f(\epsilon') + N(\omega')}{\epsilon - \epsilon' + \hbar\omega' + i\delta} \right), \end{aligned} \quad (9)$$

where f is the Fermi distribution and N is the Bose distribution function for electrons and phonons, respectively. The temperature dependence of $\Sigma(\mathbf{k}, \epsilon)$ is contained in the temperature factor of the Fermi and Dirac functions. Then the mass renormalization coefficient and the relaxation rate are given in terms of the real and imaginary part of $\Sigma(\mathbf{k}, \epsilon)$ by⁹

$$\begin{aligned} \lambda(\mathbf{k}, T, \omega) &= \int d\epsilon \frac{f(T, \epsilon) - f(T, \epsilon + \hbar\omega)}{\hbar\omega} \\ &\times \frac{M(\mathbf{k}, T, \epsilon) - M(\mathbf{k}, T, \epsilon + \hbar\omega)}{\hbar\omega}, \end{aligned} \quad (10)$$

$$\begin{aligned} \frac{\hbar}{\tau(\mathbf{k}, T, \omega)} &= \frac{1}{1 + \lambda(\mathbf{k}, T, \omega)} \int d\epsilon \frac{f(T, \epsilon) - f(T, \epsilon + \hbar\omega)}{\hbar\omega} \\ &\times [\Gamma(\mathbf{k}, T, \epsilon) + \Gamma(\mathbf{k}, T, \epsilon + \hbar\omega)]. \end{aligned} \quad (11)$$

Temperature dependence of the effective cyclotron mass is then determined by Eqs. (4), (5), (9), and (10). As can be seen in Eqs. (5), (9), and (10), $\lambda(O_{\mathbf{k}}, T)$ is an average of $\alpha_{\mathbf{k}}^2(\omega)F_{\mathbf{k}}(\omega)$ over the cyclotron orbit $O_{\mathbf{k}}$, consequently depending on the participating phonon spectrum and the cyclotron orbit under consideration. The phonon spectrum is, in general, anisotropic with respect to the crystal axes; therefore, the mass enhancement is expected to be directionally dependent. The detailed knowledge of the phonon spectrum of mercury is at present unavailable. However, the FS average $\alpha^2(\omega)F(\omega)$ deduced from the superconducting-tunneling data is shown in Fig. 1.¹⁶ The $\alpha^2(\omega)F(\omega)$ spectrum of many metals is not much different from $\alpha_{\mathbf{k}}^2(\omega)F_{\mathbf{k}}(\omega)$ (e.g., sodium⁴ and zinc¹²). Using the experimental $\alpha^2(\omega)F(\omega)$ function in mercury, Grimvall calculated the temperature dependence of the renormalization coefficient $\lambda(T)$, which first increases with temperature. The maximum is

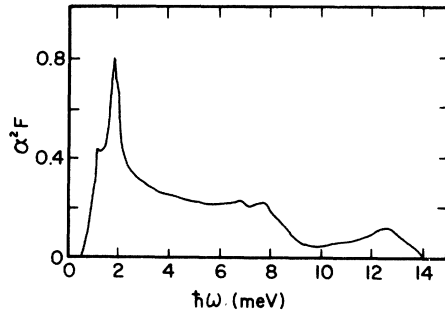


FIG. 1. Electron-phonon interaction $\alpha^2(\omega)F(\omega)$ spectrum in mercury deduced from superconducting tunneling data.

reached at a temperature T_M with $k_B T_M \approx E_t$, where E_t is the energy of the transverse phonon peak of $F(\omega)$. Since E_t corresponds to ~ 20 K, $T_M \approx 4.3$ K, and $\lambda(T_M)/\lambda_0 = 1.1$ is predicted. The relaxation time also changes with temperature and decays quickly as temperature increases. Therefore, only the region showing an increase of λ with temperature can be observed in cyclotron-resonance experiments which have to satisfy the condition $\omega\tau > 1$.

The relaxation rate is also related to $\alpha_{\mathbf{k}}^2(\omega)F_{\mathbf{k}}(\omega)$ and temperature by Eqs. (9) and (11). In the low-temperature limit, such as $k_B T \ll \hbar\omega$, $\alpha_{\mathbf{k}}^2(\omega)F_{\mathbf{k}}(\omega)$ is multiplied by a factor $e^{-\hbar\omega/k_B T}$ which decreases rapidly with the increasing frequency. Then the relaxation time is mainly dependent on the low-frequency side of the phonon spectrum, which has a parabolic shape for a Debye model. However, this part of the phonon spectrum gives negligible contribution to the mass enhancement. In the low-temperature approximation, the resulting relaxation rate is given by

$$\frac{\hbar}{\tau(\mathbf{k}, T)} \approx \frac{4\pi\hbar}{1+\lambda_0} \int_0^\infty d\omega \alpha_{\mathbf{k}}^2(\omega)F_{\mathbf{k}}(\omega) e^{-\hbar\omega/k_B T}, \quad (12)$$

where the temperature dependence of λ is neglected. Grimvall has also calculated τ using the $\alpha^2(\omega)F(\omega)$ spectrum, the FS average of $\alpha_{\mathbf{k}}^2(\omega)F_{\mathbf{k}}(\omega)$.

III. EXPERIMENTAL ASPECTS

The spectrometer employed in our experiment was a commercial Ka -band (35-GHz) Varian unit using magnetic field modulation at a frequency of 40 Hz. The sample, in the form of a thin disk, was mounted on a cylindrical TE_{113} cavity as an end wall which could be rotated around the symmetry axis of the cylinder. Details of the cavity, including the rotating mechanism, have been described previously.¹⁷

Mercury single crystals were grown in molds using high-purity mercury with the sample sur-

faces against microscope glass plates coated with a thin layer of paraffin. This coating ensured easy removal of the glass plates from the crystal. The thin and uniform coating of paraffin on the glass surfaces was accomplished by pulling glass plates at constant speed out of paraffin solution thinned with heptane in a volume ratio of 1:50. Single crystals were grown by cooling one end of the mold with liquid nitrogen with no attempt to seed crystals. The sample surface studied was nearly perpendicular to the trigonal axis. This surface seems to be easily formed in the process of crystal growing, as a very similar plane also appeared in a previous study.¹⁸

The magnetic field was supplied by a 15-in. Varian electromagnet with a Mark II Fieldial controller. The output of the temperature-regulated Hall probe of the controller was read with a digital voltmeter (DVM), and the binary-coded output of the DVM was recorded on magnetic tape. In actual experiments the magnetic field together with the signal amplitude at that field were recorded as pairs of values. Since the resonance magnetic fields are inversely proportional to the harmonic number, the field sweep was made proportional to $1/H$, so that each harmonic could be recorded with same time constant. The data were also recorded on a strip-chart recorder, as shown by a typical trace in Fig. 2.

The readout of the magnetic field from the Hall probe was calibrated with a proton NMR Gaussmeter. The calibration was performed immediately before and after each experiment by checking nine points of field, including zero field. The average of these two calibration curves was used to calibrate magnetic field readings. The field uniformity at the Hall probe and the sample position were also carefully tested. By these precautions, the uncertainty in the field reading was 0.1% at the lowest field (800 Oe) and less at higher fields.

Parallelism of the magnetic field with respect to the sample surface of mercury crystals is very important,¹⁹ especially for the temperature-dependent mass analysis. Since the data were collected over a period of time, the magnet was realigned using an optical lever consisting of 3 mirrors equivalent to a 12-m optical path. The alignment was adjusted for every experiment within 1 min of arc.

Temperature of the sample was measured using the vapor pressure of liquid helium surrounding the cavity. For the temperature range below the λ point of liquid helium, the sample cavity was immersed in the liquid-helium bath and the bath temperature was determined by a Texas Instruments precision pressure gauge. This method was not applicable above the λ point because of bubbling of liquid in the cavity. Therefore, a metallic can

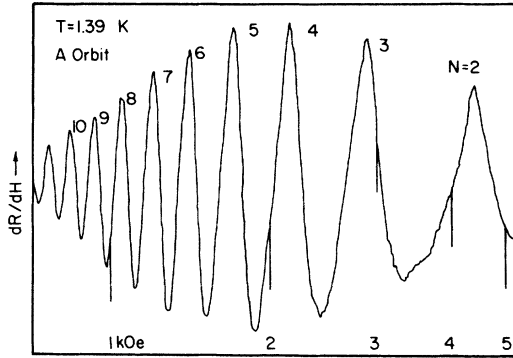


FIG. 2. Typical trace of Azbel'-Kaner cyclotron resonance in mercury. The magnetic field is swept such that the inverse field is approximately linear with time, and magnetic field markers are shown on the trace. N gives the harmonic number.

sealed with an indium O -ring was used to exclude liquid from the cavity. Mounting of the can required tedious steps with the cavity under liquid nitrogen because of the low melting point of mercury.

The helium vapor pressure was regulated by varying the conductance of the pumping line. Coarse adjustments were made manually with a vacuum valve in the main pumping line. Fine control of the conductance was made by an electrically operated feedback system using a signal from the pressure gauge. It controlled the moving coil of a 4-in. loudspeaker which had been modified to be a variable baffle in the pumping line. The stability of temperature of the bath during the recording of one trace was generally better than 0.005 K.

IV. ANALYSIS AND RESULTS

A. Azbel'-Kaner expression

In Azbel'-Kaner cyclotron resonance¹³ (AKCR), the surface impedance at the magnetic field H is given by

$$Z(H) = \alpha Z(0) \left\{ 1 - \exp \left[-2\pi i \frac{\omega}{\omega_c} \left(1 - \frac{i}{\omega\tau} \right) \right] \right\}^{1/3}, \quad (13)$$

where $Z(0)$ is the anomalous surface impedance at zero field, ω is the microwave frequency, ω_c is the cyclotron frequency, τ is the mean collision time, and α is a constant of order unity. The cyclotron frequency ω_c is related to the cyclotron effective mass by

$$\omega_c = eH/cm^*, \quad (14)$$

where c is the speed of light and m^* is the cyclotron mass. The term $i/\omega\tau$ in parentheses in Eq. (13) makes $Z(H)$ a damped oscillation due to electron scattering. The field derivative dR/dH of the

real part of $Z(H)$ is usually the experimental observable, as shown in Fig. 2. In the limit of $\omega\tau \rightarrow \infty$, the resonance fields measured at dR/dH maxima are given by

$$H_N = (cm^*\omega/e) 1/N, \quad (15)$$

where N is the harmonic number. Consequently, the cyclotron mass m^* can be determined experimentally by plotting the $1/H_N$ -vs- N relation. This simple analysis, however, depends on the value of finite $\omega\tau$ as practically encountered. The effect of the finite $\omega\tau$ shifts the field positions of dR/dH maximum according to (13), and the slope of the $1/H_N$ -vs- N plot gives different cyclotron masses for different values of $\omega\tau$. This is demonstrated in Fig. 3, which shows masses calculated using Eq. (15) for a resonance described by Eq. (13).

The resonance line shape observed in the present study is assumed to be the Azbel'-Kaner type, and the cyclotron mass is analyzed using Eq. (13) with actual values of $\omega\tau$ determined by the Haüssler-Welles method.²⁰ This process is justified by the fact that the Chambers case²¹ and the retardation effect²² do not play any important role in the present case, as can be seen in the following discussion.

In an analysis of AKCR, Chambers²¹ has considered the resonance line shape and has shown that, if relatively few electrons participate in the resonance and $\omega_c\tau \geq 50$, then AKCR line shapes are independent of the relaxation time, while the fractional linewidth $\Delta H/H_N$ is proportional to $1/\omega\tau$. This is the so-called Chambers limit. Since present experimental measurements deal with dominant resonance signals and $\omega\tau$ reaches 20 at its maximum, this limit is not applicable. However, an attempt has been made to try the Chambers line-shape analysis for some experimental data. The results indicate that the dR/dH amplitude varies

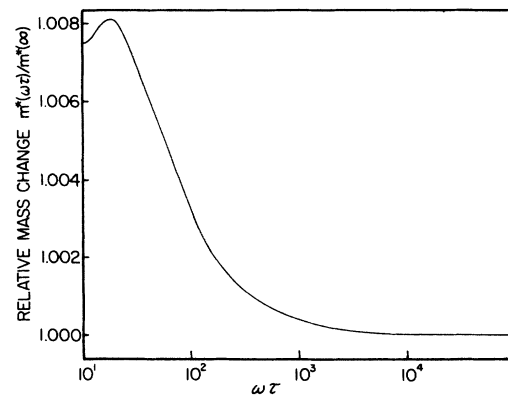


FIG. 3. Change in cyclotron mass with $\omega\tau$ determined from Eq. (15) for an Azbel'-Kaner resonance described by Eq. (13), with m^*/m_0 at $\omega\tau = \infty$ equal to 0.726.

by a factor of 3 for the first ten harmonics and $\Delta H/H_N$ changes from 0.168 to 0.053 between the third and tenth harmonic. Therefore, the Chambers analysis of $\omega\tau$ determination is not adequate for the present data.

In contrast to this limit there is the retardation effect,²² which leads to exponentially decreasing amplitudes of successive subharmonic resonances. Retardation theory applies when the time dependence of the rf field cannot be ignored while the electrons are passing through the skin layer. Then the use of Azbel'-Kaner theory determines an apparent cyclotron mass m_a^* and an apparent relaxation time τ_a^* which differ from the mass m^* and relaxation time τ by an amount which depends on retardation effects. Thus, we actually measured m_a^* and τ_a^* . The question is whether change in the retardation term resulting from the variation of $\omega\tau$ with temperature was significant in our measurements. We calculated this change for the observed range of $\omega\tau$ between 20 and 10 using Drew's²² expressions for m_a^* and τ_a^{*-1} . Values used in the calculation were Fermi velocity $v_F = 0.9 \times 10^8$ cm/sec; mean free path $l = 10^{-2}$ cm; dc conductivity $\sigma_0 = 1.5 \times 10^9 \Omega^{-1} \text{cm}^{-1}$; free-electron radius $k_F = 1.37 \times 10^8 \text{cm}^{-1}$. For a change of $\omega\tau$ from 20 to 10, the fractional change in both m_a^* and τ_a^{*-1} caused by the change in the retardation contribution was found to be $10^{-2}\%$. Thus, the apparent temperature dependence of the mass and relaxation rate from retar-

ation effects was not significant in our measurements and can be neglected for the analysis of $\omega\tau$ and m^* .

B. Cyclotron-mass results

The cyclotron mass was determined by the following steps. From the resonance pattern of dR/dH , the magnetic field of maximum dR/dH amplitudes was measured for 10 harmonics, including the fundamental, except for high-temperature data, which showed less than 10 harmonics due to the small $\omega\tau$ value. The peak positions were determined by a computer program which fitted each peak to a parabola and found the apex directly from the data recorded on the magnetic tape. This method improved the accuracy of the resonance field measurements, especially because of the non-linear sweeping of the magnetic field resulting from the $1/H$ sweep. These measured resonance fields (H'_N) did not give a straight line in the $(H'_N)^{-1}$ -vs- N plot, since the effect of the finite $\omega\tau$ shifts the resonance fields differently for harmonics with different harmonic number N . Therefore, corresponding changes of the dR/dH maxima from H_N were calculated using Eq. (13) and $\omega\tau$ values experimentally determined. The experimental values H'_N giving the dR/dH maxima of harmonics were accordingly corrected to obtain experimental H_N values. The cyclotron mass was determined from the least-squares slope of the H_N^{-1} -vs- N plot using Eq. (15).

The cyclotron mass of the electron lenses measured from the dominant resonance signal at different field directions in the sample plane is shown in Fig. 4. The threefold symmetry of these data and a comparison to previous data¹⁸ taken in the trigonal plane indicate that the sample surface is very close to the trigonal crystallographic plane. Orbits A and B on a lens are taken with the magnetic field direction at the bisectrix direction and 15° from the bisectrix direction, respectively, as shown in Fig. 4.

The temperature dependences of the cyclotron mass in mercury studied for orbits A and B are displayed in Figs. 5 and 6, respectively. The uncertainties indicated are twice the standard deviation of the mass determinations. In Figs. 5 and 6, m^* versus T^2 is plotted, and this linear plot demonstrates a T^2 dependence. According to Eqs. (9) and (10), the temperature-dependent mass re-normalization constant can be expressed to first order by⁹

$$\lambda(\vec{k}, T) = \lambda(\vec{k}, 0) + \frac{4\pi^2}{3\hbar^2} \times \int d\omega \frac{\alpha_{\vec{k}}^2(\omega) F_{\vec{k}}(\omega)}{\omega^3} (k_B T)^2. \quad (16)$$

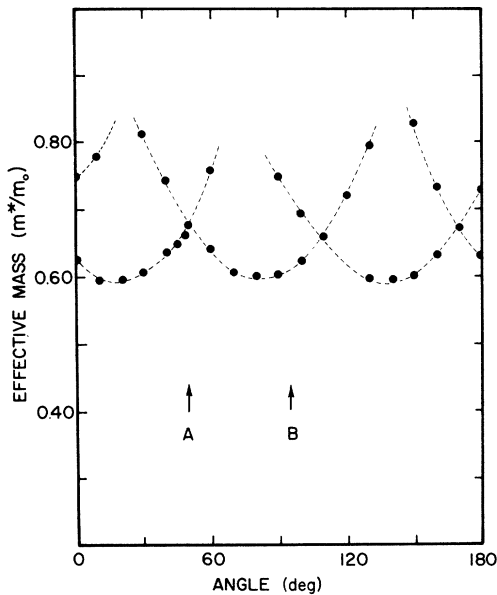


FIG. 4. Effective cyclotron mass as a function of direction of the applied magnetic field parallel to the sample surface. The field directions used for temperature-dependent measurements are indicated by arrows A and B.

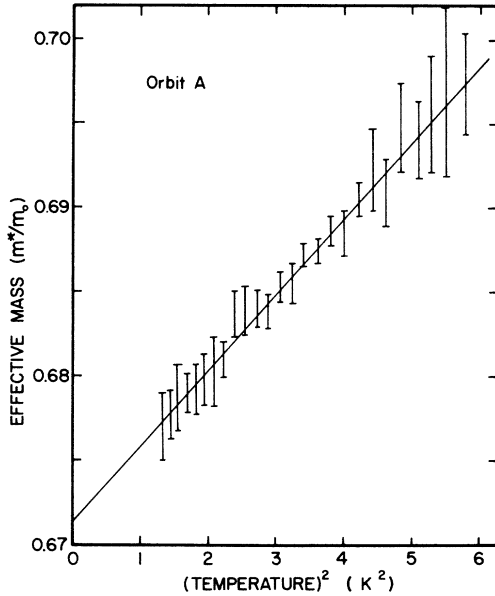


FIG. 5. Experimental cyclotron effective mass as a function of temperature squared for orbit A.

From Eqs. (4), (10), and (16) the cyclotron mass in our temperature range is given by

$$m^*(O_{\mathbf{k}}, T) = m^*(O_{\mathbf{k}}, 0) + m_b \times \left(\frac{4\pi^2}{3\hbar^2} \int d\omega \frac{\alpha_{\mathbf{k}}^2(\omega) F_{\mathbf{k}}(\omega)}{\omega^3} \right) (k_B T)^2. \quad (17)$$

Therefore, the observed temperature dependence of the cyclotron mass which can be described by

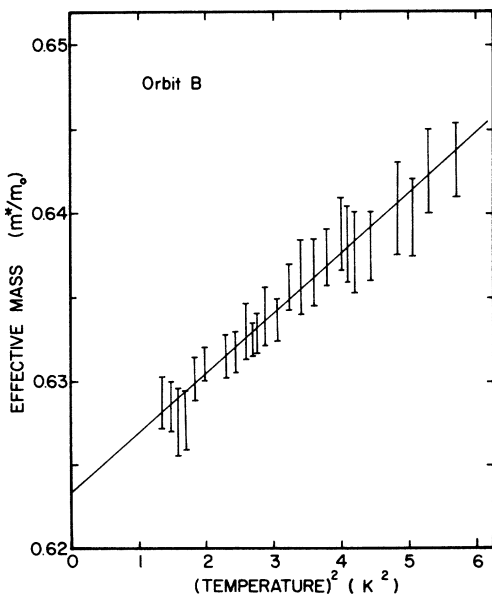


FIG. 6. Experimental cyclotron effective mass as a function of temperature squared for orbit B.

TABLE I. Zero-temperature cyclotron mass and mass-increment coefficient defined by Eq. (18).

	$m^*(0)/m_0$	$c_{\mathbf{k}}(\text{K}^{-2})$ ($\times 10^3$)
A Orbit	0.671 ± 0.002	6.8 ± 0.9
B Orbit	0.623 ± 0.002	5.7 ± 0.8
Ref. 5		3.9

$$m^*(O_{\mathbf{k}}, T) = m^*(O_{\mathbf{k}}, 0)(1 + c_{\mathbf{k}} T^2) \quad (18)$$

is in good agreement with the theory prescribing a T^2 dependence. The experimental values of $m^*(O_{\mathbf{k}}, 0)$ and $c_{\mathbf{k}}$ for the two orbits are summarized in Table I, together with the result of a previous study.⁵ The values of $c_{\mathbf{k}}$ are different for the different orbits. This indicates anisotropy in the $\alpha_{\mathbf{k}}^2(\omega)F_{\mathbf{k}}(\omega)$ spectrum, as outlined in the theory. Similar observations have also been made using the lens orbits in zinc⁷ and accounted for by an anisotropy in the phonon spectrum.¹² Using the theory of Truant and Carbotte, our results also suggest anisotropy in the phonon spectrum of mercury. The magnitude of the mass enhancement $m^*(T)/m^*(0)$ for the two orbits studied are compared with the theoretical calculation in Fig. 7. The theoretical $m^*(T)/m^*(0)$ -vs- T relation is evaluated using Eq. (4) with Grimvall's calculation⁴ of $\lambda(T)/\lambda(0)$ obtained from the $\alpha^2(\omega)F(\omega)$ function averaged over the FS. Therefore, the calcu-

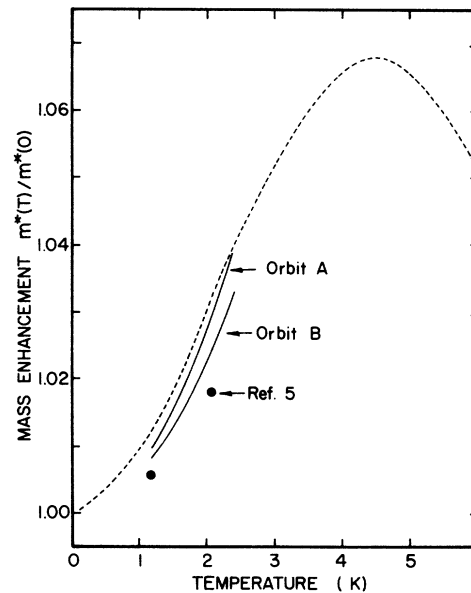


FIG. 7. Effective-mass enhancement as a function of temperature. The solid lines are experimental results and the dotted line is obtained by using Grimvall's $\lambda(T)/\lambda(0)$ curve given in Ref. 4.

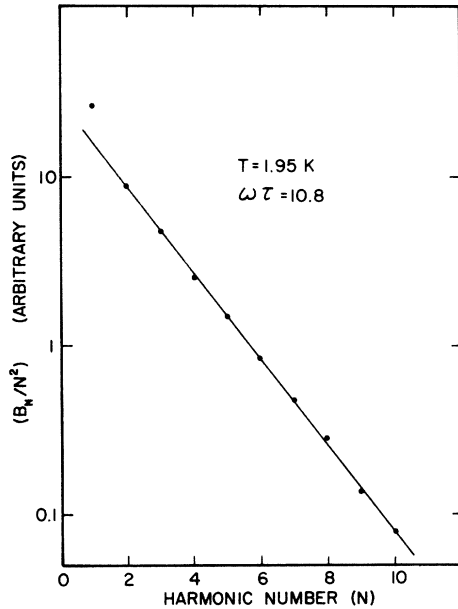


FIG. 8. Typical Häussler-Welles plot for analysis of the relaxation rate for orbit A at a temperature of 1.95 K, giving an $\omega\tau$ of 10.8.

lated $m^*(T)/m^*(0)$ is an averaged quantity. The agreement of the predicted temperature dependence with experiment in Fig. 7 is quite satisfactory, although the magnitude of the mass change does not agree.

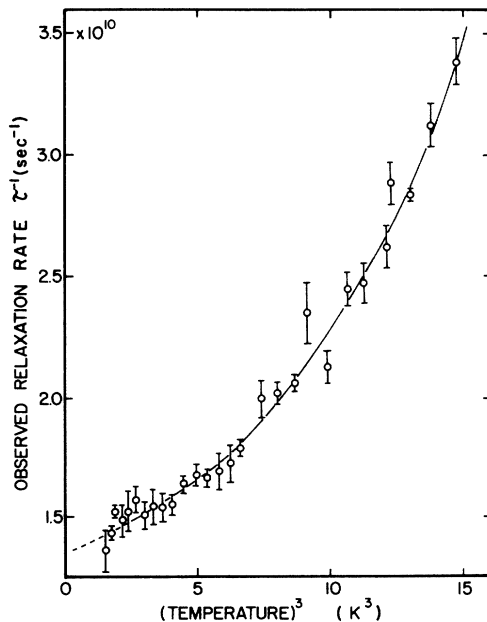


FIG. 9. Experimental relaxation rate τ^{-1} plotted as a function of T^3 for orbit A. The indicated error is twice the standard deviation in determining τ^{-1} by means of the Häussler-Welles plot.

C. Relaxation-time results

The experimental relaxation time was determined by the Häussler-Welles method,²⁰ because our resonances were dominant Azbel'-Kaner resonances with $\omega\tau$ less than 50. In this method, which is based on Eq. (13), the slope of the plot $\ln(B_N/N^2)$ versus N gives the value of $\omega\tau$ in the limit of $\omega\tau < 2\pi N$, where B_N is the dR/dH amplitude of the N th subharmonic:

$$\ln(B_N/N^2) = \text{const} - (2\pi/\omega\tau)N. \quad (19)$$

These plots were found to be linear, as shown in Fig. 8. This confirms that the method was applicable for the dominant orbits studied and that retardation effects were not observed. The observed relaxation rate τ^{-1} is plotted as a function of T^3 in Fig. 9, since the T^3 dependence is expected from Eq. (12) using a Debye model. The experimental relaxation rate τ^{-1} is the sum of contributions of the impurity and the electron-phonon part; therefore

$$\tau^{-1} = \tau_0^{-1} + \tau_{e1\text{ph}}^{-1}, \quad (20)$$

where τ_0^{-1} is the impurity relaxation rate which is a constant and $\tau_{e1\text{ph}}^{-1}$ is the electron-phonon relaxation rate. The experimental results of Fig. 9 indicate that the temperature dependence is faster than T^3 . The least-squares calculation of the temperature dependence is $T^{5.2 \pm 0.3}$. A reasonably good linear relation between τ^{-1} and T^5 is shown for the same data in Fig. 10. Therefore, the observed

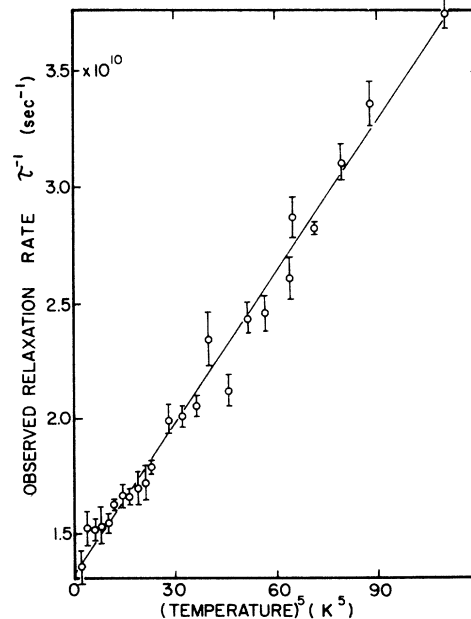


FIG. 10. Same data of τ^{-1} in Fig. 9 replotted as a function of T^5 .

TABLE II. Electronic relaxation rate due to impurities τ^{-1} and the relaxation-rate temperature factor defined by Eq. (21).

	τ_0^{-1} (sec $^{-1}$) ($\times 10^{-10}$)	$d_{\mathbf{k}}^{-1}$ (sec $^{-1}$) ($\times 10^{-8}$)
A Orbit	(1.35 \pm 0.11)	(2.05 \pm 0.17)
B Orbit	(1.29 \pm 0.15)	(1.50 \pm 0.26)
Ref. 5	(1.01 \pm 0.03)	(2.91 \pm 0.13)

temperature dependence of the relaxation rate can be expressed by

$$\tau^{-1} = \tau_0^{-1} + d_{\mathbf{k}}^{-1} T^5. \quad (21)$$

The experimental values of τ_0^{-1} and $d_{\mathbf{k}}^{-1}$ for the orbits studied are summarized in Table II, together with the results of the previous study.⁵ The magnitude of τ_0 for two orbits of the present study is practically identical, while that of the previous work is slightly bigger, indicating better quality of the first sample. The value of $d_{\mathbf{k}}$ differs for different orbits, implying that the temperature-dependent relaxation rate due to the electron-phonon interaction is dependent on the cyclotron orbit $O_{\mathbf{k}}$, as predicted by Eq. (12).

Theoretical calculations of the temperature-dependent relaxation rate using the Debye model in the low-frequency region of the $\alpha_{\mathbf{k}}^2(\omega)F_{\mathbf{k}}(\omega)$ function give the dependence⁹

$$\frac{\hbar}{\tau(\mathbf{k}, T)} = \frac{9.6\pi a_{\mathbf{k}}}{1 + \lambda(0)} [(k_B T)^3 + 0.343 \hbar \omega (k_B T)^2], \quad (22)$$

where $a_{\mathbf{k}}$ is the proportionality factor in

$$\alpha_{\mathbf{k}}^2(\omega)F_{\mathbf{k}}(\omega) = a_{\mathbf{k}}(\hbar\omega)^2. \quad (23)$$

Therefore, the theoretical temperature dependence of the relaxation rate due to the electron-phonon interaction is proportional to the cube of temperature and the constant $a_{\mathbf{k}}$, which depends on the orbit $O_{\mathbf{k}}$. The fact that the experimental temperature dependence is greater than cubic in temperature is seen both from the upward curvature of τ^{-1} versus T^3 in Fig. 9 and from the plot of τ^{-1} versus T^5 in Fig. 10. Consequently, the experimental data of the relaxation rate with temperature in the range 1.15–2.5 K confirm the previous result⁵ of $T^{4.8}$ dependence observed in mercury for the temperature region 1.15–2.1 K. The observed relaxation rate due to the electron-phonon interaction, $\tau_{\text{el,ph}}^{-1}$, and the corresponding quantity calculated by Grimvall⁴ using the $\alpha^2(\omega)F(\omega)$ function are displayed in Fig. 11. Direct comparison of the results is hardly suitable because there is little overlap of the temperature ranges treated. However, at a temperature of 2.4 K Grimvall's calculated magnitude

of the relaxation rate is about five times that of the observed one, while the experimental results of the present and previous study agree quite well.

D. Discussion of results

Experimental results of the mass change in mercury are compared with recent results from other metals in Fig. 12. The relative mass increment due to the electron-phonon interaction [$m^*(T) - m^*(0) / m^*(0)$] is plotted in Fig. 12 as a function of T^2 for mercury, lead,⁹ indium,¹⁰ and zinc.⁷ Mercury shows the steepest slope, indicating the most pronounced temperature effect. The T^2 dependence of the mass increment is well established for these metals. The slope of the T^2 plot is the experimental value of $c_{\mathbf{k}}$ defined by Eq. (18). The corresponding theoretical quantity can be deduced from Eq. (17) to give

$$c_{\mathbf{k}} = \frac{1}{1 + \lambda(\mathbf{k}, 0)} \frac{4\pi^2}{3} \left(\frac{k_B}{\hbar} \right)^2 \times \int d\omega \frac{\alpha_{\mathbf{k}}^2(\omega)F_{\mathbf{k}}(\omega)}{\omega^3}. \quad (24)$$

In order to compute the integral of the right-hand side, one must know the directional $\alpha_{\mathbf{k}}^2(\omega)F_{\mathbf{k}}(\omega)$ spectrum, which is not precisely known for many metals. However, the FS-averaged function $\alpha^2(\omega)F(\omega)$ can be experimentally determined, and Eq. (24) is approximated using $\alpha^2(\omega)F(\omega)$. Then it is given by

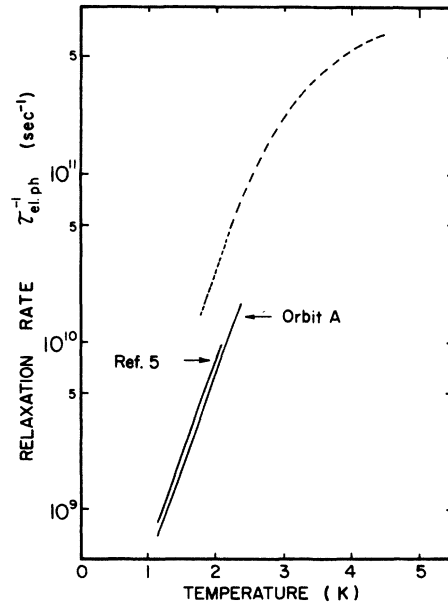


FIG. 11. Relaxation rate due to the electron-phonon interaction $\tau_{\text{el,ph}}^{-1}$ as a function of temperature. The solid lines are experimental results and the dotted line is Grimvall's calculation.

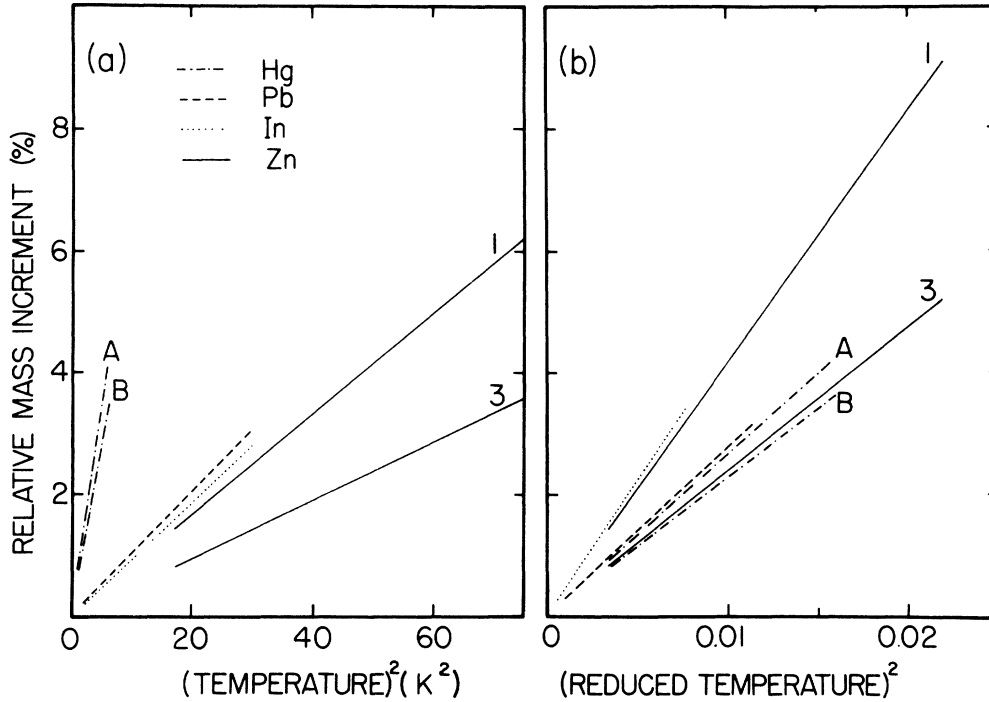


FIG. 12. Relative-mass increments due to the electron-phonon interaction for two orbits in mercury (present work), one orbit in lead (Ref. 9), one orbit in indium (Ref. 10), and two orbits in zinc (Ref. 7): (a) as a function of T^2 ; (b) as a function of $(k_B T/E_T)^2$, where E_T is the transverse phonon energy.

$$c = \frac{1}{1+\lambda(0)} \frac{4\pi^2}{3} \left(\frac{k_B}{\hbar} \right)^2 \int d\omega \frac{\alpha^2(\omega)F(\omega)}{\omega^3}. \quad (25)$$

General features of the $\alpha^2(\omega)F(\omega)$ spectrum for these materials are somewhat similar, with the lowest-frequency peak of $\alpha^2(\omega)F(\omega)$ due to transverse phonons of energy $E_t (= \hbar\omega_t)$. As a result of the sharp rise of $\alpha^2(\omega)F(\omega)$ at ω_t and the smallness of ω_t compared with the whole range of ω , the integral of Eq. (25) is heavily weighted by the contributions in the neighborhood of ω_t . Therefore, the integration may be approximated by $b/3\omega_t^2$, where b is a constant of the order unity. We have

$$[m^*(T) - m^*(0)]/m^*(0) \cong \frac{4\pi^2}{9} \frac{b}{1+\lambda_0} \left(\frac{k_B T}{E_t} \right)^2, \quad (26)$$

which is proportional to the square of the reduced temperature $k_B T/E_t$. The values of E_t/k_B are 20, 51, 69, and 71 K for mercury, lead, indium, and zinc, respectively. The experimental results are plotted as a function of the square of the reduced temperature in Fig. 12(b). Near-superposition of the slopes is obtained for mercury and lead, in good agreement with Eq. (26), because these two metals have almost identical values of λ_0 : 1.6 for mercury and 1.5 for lead. High slopes of indium and zinc compared with those of mercury and lead can be understood in terms of the small values of λ_0 , the mass renormalization coefficient

at 0 K.

The temperature dependence of the relaxation rate is interesting because the temperature dependence using a Debye model for the phonon spectrum is cubic. The relaxation rate was previously found to vary as $T^{4.8}$ in mercury,⁵ T^3 in lead,⁹ and faster than T^3 in indium.¹⁰ Thus there is considerable evidence for noncubic behavior. According to Eq. (12), this gives information about the $\alpha^2(\omega)F_{\mathbf{k}}(\omega)$ spectrum—in particular, the low-energy region. A temperature dependence different from cubic arises when the part of $\alpha^2(\omega)F_{\mathbf{k}}(\omega)$ effectively contributing to the relaxation rate is nonquadratic. This is evident in Fig. 11 for the calculated rate above 3.5 K. The observed noncubic dependence at low temperatures indicates that $\alpha^2(\omega)F_{\mathbf{k}}(\omega)$ for the orbits studied is nonquadratic at low energies, as is usually assumed using a Debye model. Unfortunately, the low-energy portion of $\alpha^2(\omega)F(\omega)$ is not determined by tunneling spectroscopy. Other experiments or calculation of the phonon density of states are required to determine the shape of $\alpha^2(\omega)F(\omega)$ at low energies for quantitative comparison with the present results.

V. CONCLUSION

The strength of the electron-phonon interaction depends upon the energy of the quasiparticle measured from the Fermi level. Since a finite tem-

perature broadens the Fermi level, the effective mass and the electronic relaxation time depend upon the temperature of the cyclotron-resonance experiment. Experiments have been carried out with mercury, which has a strong electron-phonon interaction ($\lambda_0 = 1.6$) and very-low frequency phonons ($E_t/k_B \approx 20$ K). The effective cyclotron mass and relaxation time were determined with AKCR experiments in the temperature range 1.1–2.5 K at a fixed frequency of 35 GHz for two different orbits on the electron lens. Experimental mass variations are found to be proportional to the temperature squared for both orbits, as predicted by the theory of the electron-phonon interaction. The relative mass increments, however, are different for two orbits studied, supporting the view that the directional $\alpha_{\vec{k}}^2(\omega)F_{\vec{k}}(\omega)$ for a particular cyclotron orbit $O_{\vec{k}}$ is the relevant quantity. The electronic relaxation times measured for the two orbits de-

crease rapidly with increasing temperature. The relaxation rate is found to vary as $T^{5.2 \pm 0.3}$. This confirms previous experimental results, but does not agree with the simple theory, which predicts a T^3 dependence.

ACKNOWLEDGMENTS

The authors wish to thank J. P. Carbotte and R. G. Poulsen for useful discussions, R. J. Douglas for his interest and help during the experiments and for reading the manuscript, and Buil Mah for his help in data analysis. Thanks are also extended to C. Verge for technical assistance, especially for constructing the pressure-regulating device. Research support from the National Research Council of Canada and the Dong-A Natural Science Commission of Korea (to S. H. C.) is gratefully acknowledged.

*Work supported by the National Research Council of Canada and in part by the Dong-A Natural Science Commission of Korea.

†Permanent address: Department of Physics, Korea University, Seoul, Korea.

¹S. Nakajima and M. Watabe, *Prog. Theor. Phys.* **29**, 341 (1963); *Prog. Theor. Phys.* **30**, 271 (1963); *Prog. Theor. Phys.* **30**, 772 (1963).

²J. W. Wilkins, *Observable Many Body Effects in Metals* (Nordita, Copenhagen, Denmark, 1968).

³H. Scher and T. Holstein, *Phys. Rev.* **148**, 598 (1966).

⁴G. Grimvall, *J. Phys. Chem. Solids* **29**, 1221 (1968); *Phys. Kondens. Materie* **9**, 283 (1969).

⁵R. G. Poulsen and W. R. Datars, *Solid State Commun.* **8**, 1969 (1970).

⁶P. Goy and G. Weisbuch, *Phys. Rev. Lett.* **25**, 225 (1970).

⁷J. Sabo, *Phys. Rev. B* **1**, 1325 (1970).

⁸P. Goy, *Phys. Lett.* **31A**, 584 (1970).

⁹P. Goy and B. Castaing, *Phys. Rev. B* **7**, 4409 (1973).

¹⁰P. Goy and B. Castaing, in *Proceedings of the Thirteenth International Low Temperature Conference*, edited by R. H. Kropshot and K. O. Timmerhaus (University of Colorado Press, Boulder, Colo., 1972).

¹¹P. B. Allen and M. L. Cohen, *Phys. Rev. B* **1**, 1329 (1970).

¹²P. T. Truant and J. P. Carbotte, *Solid State Commun.* **9**, 1621 (1971).

¹³M. Y. Azbel' and E. A. Kaner, *J. Phys. Chem. Solids* **6**, 113 (1958).

¹⁴S. H. Choh and W. R. Datars, *Phys. Canada* **27**, 62 (1971).

¹⁵S. H. Choh, *New Phys.* **12**, 119 (1972).

¹⁶W. L. McMillan and J. M. Rowell, in *Superconductivity*, edited by R. D. Parks (Marcel Dekker, New York, 1969).

¹⁷R. G. Poulsen and W. R. Datars, *Phys. Rev. B* **4**, 4202 (1971).

¹⁸A. E. Dixon and W. R. Datars, *Phys. Rev.* **175**, 928 (1968).

¹⁹R. G. Poulsen, Ph.D. thesis (McMaster University, 1970) (unpublished).

²⁰P. Häussler and S. J. Welles, *Phys. Rev.* **152**, 675 (1965).

²¹R. G. Chambers, *Proc. Phys. Soc. Lond.* **86**, 305 (1965).

²²H. D. Drew, *Phys. Rev. B* **5**, 360 (1972).